Published in final edited form as:
Bone. 2013 December ; 57(2): 455–467. doi:10.1016/j.bone.2013.09.007.

The Plastic Nature of the Human Bone-Periodontal Ligament-Tooth Fibrous Joint

Sunita P. Ho[*], **Michael P. Kurylo**[#], **Kathryn Grandfield**[#], **Jonathan Hurng**, **Ralf-Peter Herber**[1], **Mark I. Ryder**[2], **Virginia Altoe**[3], **Shaul Aloni**[3], **Jian Q. (Jerry) Feng**[4], **Samuel Webb**[5], **Grayson W. Marshall**, **Donald Curtis**, **Joy C. Andrews**[5], and **Piero Pianetta**[5]

Division of Biomaterials and Bioengineering, Department of Preventive and Restorative Dental Sciences, University of California San Francisco, San Francisco, CA

[1]Divisions of Orthodontics, Department of Orofacial Sciences, University of California San Francisco, San Francisco, CA

[2]Division of Periodontics, Department of Orofacial Sciences, University of California San Francisco, San Francisco, CA

[3]Materials Science Division, The Molecular Foundry, Lawrence Berkeley National Laboratory, Berkeley, CA

[4]Biomedical Sciences, Baylor College of Dentistry, Texas A&M, Dallas, TX

[5]Stanford Synchrotron Radiation Lightsource, SLAC National Accelerator Laboratory, Menlo Park, CA

Abstract

This study investigates bony protrusions within a narrowed periodontal ligament space (PDL-space) of a human bone-PDL-tooth fibrous joint by mapping structural, biochemical, and mechanical heterogeneity. Higher resolution structural characterization was achieved via complementary atomic force microscopy (AFM), nano transmission X-ray microscopy (nano-TXM), and micro tomography (Micro XCT™). Structural heterogeneity was correlated to biochemical and elemental composition, illustrated via histochemistry and microprobe X-ray fluorescence analysis (μ-XRF), and mechanical heterogeneity evaluated by AFM-based nanoindentation. Results demonstrated that the narrowed PDL-space was due to invasion of bundle bone (BB) into PDL-space. Protruded BB had a wider range with higher elastic modulus values (2-8 GPa) compared to lamellar bone (0.8-6 GPa), and increased quantities of Ca, P and Zn as revealed by μ-XRF. Interestingly, the hygroscopic 10-30 μm interface between protruded BB and lamellar bone exhibited higher X-ray attenuation similar to cement lines and lamellae within

[*]To whom correspondence should be addressed: Sunita P. Ho, Ph.D., Division of Biomaterials and Bioengineering, Department of Preventive and Restorative Dental Sciences, 707 Parnassus Avenue, University of California San Francisco, CA 94143, sunita.ho@ucsf.edu, Phone: 415-514-2818.
[#]both authors contributed equally.

bone. Localization of the small leucine rich proteoglycan biglycan (BGN) responsible for mineralization was observed at the PDL-bone interface and around the osteocyte lacunae. Based on these results, it can be argued that the LB-BB interface was the original site of PDL attachment, and that the genesis of protruded BB identified as protrusions occurred as a result of shift in strain. We emphasize the importance of bony protrusions within the context of organ function and that additional study is warranted.

Keywords

bone-PDL-tooth fibrous joint; periodontal ligament; alveolar bone; bundle bone; bone functional adaptation; discontinuities

1. INTRODUCTION

Operating under Wolff's principles of organ use and disuse, the bone-periodontal ligament (PDL)-tooth fibrous joint and its respective tissue components react to occlusal inputs, that is, physiological and/or non-physiological loads. As such, the tissues adapt to functional demands, a cycle which may continue in perpetuity under prolonged loading. It is proposed that optimal function of the system is preserved by a characteristic functional PDL-space of 150–380 μm [1], maintained via balance of anabolic and catabolic activity of bone, and equivalent turnover of the PDL and lamellar cementum deposition [2] in response to the stress and strain fields generated during function.

Ideally, the occlusal loads placed on the tooth should result in the external architecture of the tooth to form a geometric conformity with bone and vice versa, under loaded conditions. The tooth is subjected to a variety of loads and when the majority of the compressive loads align with the anatomical axis of the tooth, the PDL could undergo shear, a mixed mode of tension and compression strain fields, supplemented by flexural moments at the tethered ends of the ligament, i.e. the radial PDL-inserts within bone and cementum [3]. As described by D'Arcy Thompson, force fields within organs and tissues promote the internal architecture [4]. In addition, Wolff's fundamental law of bone remodeling states that changes in the internal architecture of bones, when pathophysiologically altered (e.g. via extraneous loading or increased frequency of loading), can change the overall form of bone [5]. Bone cells are capable of adapting to local mechanical stresses via feedback loops, remodeling and modeling micro and macro-structural changes to remain "functional" bone, despite existing in a pathological state [5]. As a result, it seems inevitable that tissues and their interfaces adapt towards a pathological state to accommodate the significant shifts in loads and frequencies.

Previous studies have demonstrated, at a macroscale, heterogeneous composition in the form of physicochemical gradients within normal bone-PDL-tooth specimens [6]. It has been proposed that the graded interfaces within a joint consisting of uniform PDL-space can optimize distribution of functional loads, thus promoting functional life of the organ. Interestingly, in our recent study we demonstrated the presence of mechanical, structural, and chemical discontinuities (abrupt transitions between two dissimilar materials), localized at the alveolar bone-PDL and cementum-PDL interfaces within the complex [6]. Sharp

gradients in the form of elastic discontinuities were observed within bone at the lamellar and protruded bone interface. These protruded sites manifesting as elastic discontinuities can be regions of high stress localization in a load-bearing complex. As such, the complex is conducive to amplified strains and stresses leading to perpetuation of the discontinuous interfaces while still maintaining function. Results in this study also raise the question that if organs are predisposed with discontinuities, should therapeutic loads be imposed? While functional load adaptation have been described in skeletal orthopedics [7-12], to our knowledge there exist no studies on bone-PDL-tooth fibrous joint adaptations within oral and craniofacial orthopedics.

The goal of this study is to illustrate characteristics of the narrowed PDL space within the bone-PDL-tooth complex. The elastic graded properties of the inter-lamellae, and lamellae of lamellar bone, bundle-lamellar bone interface and bundle bone of a fibrous joint will be reported within the context of organ function by using erupted and undiseased specimens extracted from humans. This is because; a combination of matrix structure, biochemical and elemental composition, and elastic modulus of various tissues could affect biomechanical function. Hence, detailed PDL-bone, PDL-cementum and protruded bone-lamellar bone integration at the 5-50 μm wide reduced complex will be discussed based on evaluations using various complementary higher resolution characterization techniques, such as atomic force microscopy (AFM), nano X-ray computed tomography (nano- TXM), microprobe X-ray fluorescence imaging (micro-XRF) and AFM-based nanoindentation.

2. MATERIALS AND METHODS

Specimens for Micro XCT™ imaging and physicochemical characterization

Specimens (N = 10) were acquired from patients undergoing orthodontic treatment where teeth along with proximal bone were removed. Teeth were removed due to crowding of dentition. Inclusion criterion for a specimen was proximal bone in the coronal half of the extracted tooth. Exclusion criteria were specimens with caries, periodontal disease, and/or root resorption. The protocol was approved by the UCSF Committee on Human Research. Specimens were sterilized using 0.31 Mrad of γ-radiation [13] and each specimen was scanned using a micro-X-ray computed tomography unit (μ-XCT, Micro XCT-200, Pleasanton, CA) [3]. The mandibular-molar complex was then imaged using a μ-XCT [3] to identify tooth-alveolar bone association when compressed with a finite load. Five specimens were used for immunohistochemistry and histology. Another five specimens were used for AFM, which were also used for site-specific mechanical properties using AFM-based nanoindentation and X-ray microprobe techniques. Thin-sectioned specimens (1-5 μm thickness) were prepared out of the remaining specimens and mounted on 100 nm think silicon nitride (Si_3N_4) membranes for nano-TXM. It should be noted that specimens were taken from the root using the first two-thirds for acellular cementum and last one-third for secondary cementum as location indicators [14].

2.1. Deparaffinized sections for conventional histology and immunohistochemistry

Extracted molars (N = 5) containing PDL and alveolar bone were prepared for histology as stated in our previous work [6]. The sections were subsequently stained with hematoxylin

and eosin (H&E) and picrosirius red (PSR). Stained tissues were characterized for structural orientation and integration of the PDL with bone and cementum, using a polarized light microscope (BX 51, Olympus America Inc., San Diego, CA) to enhance the birefringence of collagen in alveolar bone and cementum. Images were acquired using Image Pro Plus v6.0 software (Media Cybernetics Inc., Silver Springs, MD).

2.2. Antibody tagging and localization

Antibody tagging was performed using the procedures established and described in our previous works [3]. In brief, the small leucine rich proteins (SLRPs), biglycan (BGN) and fibromodulin (FMOD) within alveolar bone, periodontal ligament (PDL), bone-PDL and cementum-PDL entheses were identified following deparaffinization of mounted sections with xylene. Antigen retrieval was performed using trypsin digestion [3]. The following modifications to the manufacturer's protocol were made: FMOD, BGN stains, and respective antibodies from polyclonal rabbit sera were acquired from Dr. Larry Fisher (NICDR/NIH, Bethesda, MD). Specimens were blocked at room temperature for 20 min in 1% bovine serum albumin (Sigma, St. Louis, MO), 1.5% mouse serum (Sigma, St. Louis, MO) in PBS. Antibody incubation was then performed overnight (18 h) at 4 °C, with the appropriate antibody diluted in blocking solution (1:50 for anti-BGN, 1:100 for anti-FMOD). Slides were washed 3 times the following day in PBS for 5 min each. Secondary antibody incubation of mouse anti-rabbit-IgG conjugated to HRP (Sigma, St. Louis, MO), diluted 1:100 in blocking solution, was performed at room temperature for 30 min, and then washed 3 times in PBS 10 min each.

3,3′-Diaminobenzidine (DAB) Enhanced Liquid Substrate System (Sigma, St. Louis, MO) was used per manufacturer's instructions with an incubation of 1 h to provide a brown coloration of epitope locations. The specimens were then counterstained with Gill's III Hematoxylin (Sigma), dehydrated through serial solutions of 80% alcohol, 95% alcohol, 100% alcohol, and xylene, and mounted with Permount (Sigma). An Olympus BX51 light microscope was used for imaging with analyses using Image Pro software (Media Cybernetics Inc., Bethesda, MD).

2.3 AFM, AFM-based nanoindentation, and μ-XRF characterization

Light microscopy (BX 51, Olympus America Inc., San Diego, CA) was used to image the surface of ultrasectioned block specimens [15] (N = 5), to identify bundle and lamellar bone in alveolar bone, and cementum of the tooth. Block specimens were characterized using an AFM, AFM-based nanoindentation and microprobe for micro-XRF. Light micrograph image acquisition and analysis of lamellar bone (specifically interlamellae and lamellae regions), and bundle bone were conducted using Image Pro Plus v6.0 software (Media Cybernetics Inc., Silver Springs, MD).

2.3.1. AFM for structural analysis—Semi-qualitative data representative of bundle-lamellar (LB-BB) bone interface, collagen periodicity, hygroscopicity of inter-lamellae, and PDL-inserts within bundle bone was performed using contact mode AFM (Nanoscope III, Multimode; DI-Veeco Instruments Inc., Santa Barbara, CA) under dry and hydrated

conditions [16]. AFM micrographs were analyzed with Nanoscope III version 5.12r3 software (Nanoscope III, Multimode; DI-Veeco Instruments Inc., Santa Barbara, CA).

2.3.2. AFM-based nanoindentation for site-specific mechanical property evaluation—Nanoindentation was performed on the ultrasectioned block specimens using an AFM attached to a load displacement transducer (Triboscope, Hysitron Incorporated, Minneapolis, MN). A sharp diamond Berkovich indenter with a conventional radius of curvature less than 100 nm (Triboscope, Hysitron Incorporated, Minneapolis, MN) was fitted to the transducer. Site-specific measurements of reduced elastic modulus (E_r) in cementum, PDL, bundle, and lamellar bone were made under wet conditions using a displacement control mode and a penetration depth of 500 nm, with a load, hold, and unload for 3s each. Fused silica was used to calibrate the transducer under dry and wet conditions [16-20].

2.3.3. Nano-TXM for structural analysis—Five extracted bone-tooth specimens were sectioned into 3 × 3 × 3 mm cubes using a diamond wafering blade and a low-speed saw (Isomet, Buehler, Lake Bluff, IL) under wet conditions. Specimens were mounted on AFM steel stubs (Ted Pella, Inc., CA) using epoxy and were ultrasectioned with a diamond knife (MicroStar Technologies, Huntsville, TX) to isolate 1-5 μm thick specimens. Nano-scale structural properties of mineralized tissue in bone-PDL-tooth sections mounted on Si_3N_4 membranes were determined by transmission X-ray microscopy (TXM) (Xradia, Pleasanton, CA) images collected at the Stanford Synchrotron Radiation Lightsource (SSRL) beamline 6-2 [21]. Absorption images of specimens were performed at a X-ray energy of 5.4 keV using monochromatic X-ray radiation. Samples were mounted orthogonal to the incident X-ray beam with transmitted x-rays imaged on a transmission detector system comprised of a scintillator optically coupled by a 10X objective to a 1024 × 1024 pixel Peltier-cooled CCD detector. Zernike phase contrast to enable imaging low-Z materials was achieved by the addition of a 3.0 μm thick nickel phase ring [21].

2.4. Micro-XRF mapping of ultrasectioned specimens

Elemental distribution and localization within bone-PDL-tooth block specimens were determined by X-ray fluorescence images collected at the SSRL beam line 2–3. Data were acquired with incident X-ray energy of 12 keV, which was set by using a Si (111) double crystal monochromator [6]. The fluorescence lines of calcium (Ca), phosphorus (P), and Zinc (Zn) within the alveolar bone and cementum were monitored using a silicon drift Vortex detector (SII NanoTechnology USA Inc.). The microfocused beam of 2 × 2 μm was provided by a Pt-coated Kirkpatrick-Baez mirror pair (Xradia Inc.) The incident and transmitted x-ray intensities were measured with nitrogen-filled ion chambers. Specimens were mounted at 45 degrees to the incident x-ray beam and were spatially rastered with the microbeam using a Newport VP-25XA-XYZ stage. Additionally, the entire fluorescence spectrum was also collected at each data point. Using a beam exposure of 100 ms per pixel high resolution maps were generated with scanning step size of 1 μm.

2.5. Transmission Electron Microscopy (TEM) of ultramicrotomed sections

90 nm thick ultramicrotomed sections, corresponding to the surface of sections studied by TXM, were coated with a thin (~5 nm) layer of carbon and analyzed in a JEOL 2100F Field Emission TEM operated at 120 keV. Conventional bright-field TEM images and high-angle annular dark-field (HAADF) scanning TEM (STEM) images with compositional contrast [22] were recorded. High-resolution TEM (HRTEM) was utilized to visualize lattice fringes representative of crystalline structure. The crystallinity and texture of lamellae and interlamallae regions was analyzed with selected-area electron diffraction (SAED) patterns.

3. RESULTS

3.1 Qualitative assessment of non-conforming surfaces revealed with Micro XCT™ imaging

Micro XCT™ 2D images of intact bone-PDL-tooth fibrous joint specimens provided two types of tissue associations within the joints that were qualitatively assessed: 1) conforming (complementing) tooth root and alveolar bone surfaces and 2) non-conforming root and bone surfaces characterized by the presence of protrusions contiguous with alveolar bone, “encroaching” into the PDL-space. Despite the presence of bony protrusions (Fig. 1), *in situ* images of the periodontium under no load illustrated a seemingly uniform functional PDL-space. While under loaded conditions, a qualitative observation of nonconforming root and bone surfaces was made. Loaded conditions illustrated narrowed PDL-space, highlighted by focal contacts of non-conforming tooth root and alveolar bone surface sites (Figs. 1C & D). It should be noted that cementum on the tooth root surface also demonstrated protrusions into the PDL-space.

3.2 Structural and biochemical heterogeneities identified with various imaging modalities and immunohistochemistry

High magnification light microscopy images of ultrasectioned compromised bone-PDL-tooth specimens illustrated distinct structural constructs within cementum, PDL, and alveolar bone at narrowed/constricted PDL sites (Figs. 2A & B). Picrosirius red staining coupled with polarized light microscopy of lamellar bone (LB) demonstrated differential collagen fiber orientation between lamellae and interlamellae regions of lamellar bone characterized by birefringence (Fig. 2D). Similarly, within secondary cementum of the tooth root, structural heterogeneity in the form of lamellar and non-lamellar structures was identified with non-lamellar secondary cementum interfacing with the PDL-space (Fig. 2C). Within alveolar bone two regions distinguished by differential collagen fiber orientation were identified using hematoxylin and eosin staining (H&E) coupled with polarized light microscopy (Figs. 2E & F). Bony protrusions adjacent to the PDL-space, which demonstrated primarily radial fibers, were identified as bundle bone (secondary) interfacing circumferential collagen fibers characteristic of (primary) lamellar bone. Interestingly, H&E staining demonstrated directional bone growth illustrated by bony protrusions expressed at the PDL- alveolar bone entheses, however this was not observed at the cementum-PDL entheses (Figs. 2G & H).

Composite atomic force micrographs of the surface of sectioned protruded bone-PDL-tooth block specimens acquired under wet and dry conditions illustrated radial fibers insertions sites within mineralized protrusions of both bundle bone and cementum at respective tissue entheses (Fig. 3A). Two structurally distinct regions were again demonstrated within alveolar bone characterized by an abrupt structural transition from radially oriented Sharpey's fibers to circumferential lamellar bone, with bundle bone exhibiting more hygroscopic nature than lamellar bone, suggestive of differential degrees mineral and organic content (Fig. 3B). Numerous osteocyte lacunae were also noted at the LB-BB interface, in conjunction with the insertion of Sharpey's fibers across BB and into the LB region (Fig. 3C). Additionally, within lamellar bone, inter-lamellae regions demonstrated greater hygroscopic nature, with increased swelling as compared to the lamellae. Interestingly, macroscale AFM scans in wet conditions illustrated a third structurally unique region characterized by hygroscopic network of transitioning radial-circumferential fibers within the lamellar bone-bundle bone interface (LB-BB) interface (Fig. 3).

Immunohistochemistry labeling for fibromodulin (FMOD) demonstrated localization of FMOD in Sharpey's fibers of bundle bone (BB), cementum, PDL, vascular tissue, and within lamellar bone (LB) localizing as striations bordering alveolar bone vasculature spaces (Figs. 4A & B). Tooth-PDL-bone histology sections labeled for biglycan (BGN) illustrated localization at the alveolar bone-PDL tissue interface, commonly known as entheses, regardless of the presence or absence of protruded bundle bone (Fig. 4C). BGN localization at the cementum-PDL entheses was also observed (Fig. 4D).

X-ray absorption maps of thin bone-PDL-tooth specimens (1-5 μm) collected via nano-transmission X-ray Tomography (Nano-TXM) illustrated various attenuating regions within protruded alveolar bone (Fig. 5). Bony protrusions adjacent to the PDL-space were identified as bundle bone (BB) by the presence of hygroscopic organic inserts (Sharpey's fibers) confirmed by high-resolution atomic force microscopy (AFM) under wet conditions. AFM also demonstrated hygroscopic radial PDL fibers in BB changed orientation into circumferential in LB at the interface between lamellar bone and bundle bone. Interestingly, this region of fiber orientation transition, or interface, corresponded with a 10-30 μm wide junction between BB and LB which exhibited higher X-ray attenuation. Additionally, alternating bands of higher and lower attenuating regions corresponding with lamellae and inter-lamellae regions of lamellar bone were also identified.

Further investigation of these regions with Transmission Electron Microscopy (TEM) in both conventional bright-field (Figs. 6A & B) and HAADF STEM compositional contrast images (Fig. 6D) demonstrated the alternating lamellae and inter-lamellae spaces. The periodic 67 nm collagen banding pattern, characteristic of Type I collagen, is evident in both lamellae and interlamellae regions (Fig. 6B). High-resolution micrographs (Fig. 6C) exhibited lattice fringes characteristic of a crystalline mineral phase, while selected area electron diffraction patterns (Fig. 6E) confirm both the crystalline nature of the lamellae and interlamellae regions and their respective preferential orientation (texture), as indicated by the 002 arcs corresponding to the alignment of the crystal's c-axis.

3.3. Elemental composition by mapping X-ray fluorescence of Ca, P, and Zn using microprobe

High resolution microprobe X-ray fluorescence spectroscopy of elemental Calcium (Ca), Phosphorus (P), and Zinc (Zn) (Fig. 7) demonstrated higher X-ray fluorescence counts of Ca and P in bony protrusions identified as bundle bone (BB) relative to the interfacing lamellar bone (LB). Line maps illustrated steep chemical gradients in Ca and P from LB to BB, originating at the LB-BB interface. Interestingly, a distinct localization of Zn, an element theorized as a potential marker for function- and disease-induced biomineralization, was noted in BB.

3.4. Mechanical gradients from AFM-based nanoindentation

Site specific nano-indentation of lamellar bone (LB) and adjacent bundle bone (BB) demonstrated significantly higher elastic moduli (E_r) in bundle bone relative to lamellar bone, ranging from 2-8GPa, and 0.8-6GPa, respectively. It should be noted that due to the heterogeneous architecture and composition of the material, mechanical properties were reported as a range of values rather than an averages as illustrated via frequency plot (Fig. 8). Multiple line profiles starting from LB demonstrated a steep mechanical gradient from LB into BB (Fig. 8). Interestingly, from a mechanics perspective, the LB-BB interface is representative of a discontinuous interface, interfaces which are known to accumulate local strain amplification and subsequent mechanical failure.

4. DISCUSSION

In this investigation, the bone-PDL-tooth complex illustrated bony protrusions with physicochemical discontinuities. The structural phenotype of bundle bone is not typical of development, but is related to the latter stages of the organ when it comes into function (i.e. mastication) [14, 24-27] during which time mechanical loads are felt by the bone-ligament-tooth complex. Bone continuously adapts to accommodate mechanical loads identifying the “functional plasticity” of alveolar bone [14, 24-27]. Regardless, adaptation over time prompts a uniform periodontal ligament space of 150-380 μm [1, 3] which constitutes an optimum range of motion for the tooth inside the alveolar socket. However, bone growth of human dentition presented previously [6] and in this study hypothesizes a cause for bony protrusions from the lamellar bone that at the very least are unique sites that warrant investigation. Hence, the logical questions are: 1) What features are suggestive of functional adaptation of the fibrous organ? And of further importance: 2) Is there a critical point at which adaptation restricts or prevents organ function shifting it to a state of pathology? From a philosophical stand-point, where is the balance between adaptation and pathology and as adaptation occurs does that mean that the potential for adaptation decreases, or when the organ crosses a critical threshold does the next effort at adaptation lead to destruction?

Addressing the first question we made a qualitative observation of a change in tooth-alveolar bone association, i.e. the geometric conformation at no load that became nonconforming when loaded (Fig. 1). This observation highlighted the potential for nonconforming regions to experience strain amplification when under load. Hence it is plausible that the protrusion sites (stars in Fig. 1) act as potential culprits that shift the organ into malfunction. Sites that

promote an irregular functional space of less than 100 μm are not to be confused with “hot spots” (strain amplified sites) when functional loads are well within physiological limits and bone-tooth geometric conformation is maintained [23]. The observations presented in this study raise specific questions; “How are these nonconforming regions or protrusions generated? What is the physicochemical makeup of these protrusions when compared to primary lamellar alveolar bone?” The first question can be systematically answered using animal models, but does not fall within the scope of this study. However, it is the second question that will be answered by discussing the measured graded physicochemical properties of the protruded bone-lamellar bone interface in a human bone-PDL-tooth fibrous joint.

The accepted theory on bone adaptation is driven by the reduction of resultant strain fields from dynamic mechanical loading [4]. According to Wolff “form follows function and that change in the internal architecture of bones deformed and stressed pathologically, entail secondary alterations in the external form of these bones, also following mathematical rules”. Additionally, the “development of an external shape which Roux later called “functional” occurs to meet functional demands; however, could have shifted the tissue and/or organ to a pathological state” [5]. Extending these concepts to alveolar bone, we speculate that the bony protrusions could occur due to nonphysiological functional demands at the tethered ends of the PDL-bone and PDL-cementum interfaces. The response to the shift in strain at the interfaces can be identified by tipping of the blastic and clastic events thus forming or resorbing mineral along the PDL-bone and PDL-cementum tethered ends, within bone *per se*, and that these local events strengthen the region to accommodate functional demands.

In this study, the pullout forces at the tethered ends are best evidenced by the hematoxylin and eosin histology sections (Fig. 2E & F). These sections demonstrated microscale protrusions, presence of basophilic groups at the PDL-bone and PDL-cementum attachment sites, and established a positive correlation with the presence of FMOD and BGN biomolecules at similar anatomical locations (Figs. 2, 4). It is proposed that BGN prompts mineralization at the soft-hard tissue attachment site [28] in the direction of the stretched PDL fibers. The direction of the PDL-inserts in the protruded bone, i.e. bony protrusions are indicative of the directional stretch of original fibers, and may have prompted bone lining cells to produce mineral along the strained fibers. This of course should not come as a surprise because of the historic postulation that cortical bone formation occurs along the tension based strain profiles [4].

Within the bone-PDL-tooth fibrous joint, the pullout forces at the soft-hard tissue interfaces are the mechanobiologically active sites. Also known as enthesis organs in orthopedics, the interfaces have an integral role in maintaining organ-level biomechanics [8]. Most often a reductionist approach is sought, and interfaces by themselves are interrogated, with various state-of-the-art instrumentation. While the reductionist approach is necessary and can provide a clearer picture of the interfaces alone, this approach by itself fails to answer the impact of intrinsic characteristics of an interface on overall organ function. As stated by D’Arcy Thompson, “the beauty and strength of the mechanical construction lie not in one part or in another, but in the harmonious concatenation which all the parts, soft and hard,

rigid and flexible, tension-bearing and pressure-bearing, make up together" [4]. Applying D'Arcy's principle to the bone-PDL-tooth complex, there exist many tissues and their interfaces in this fibrous joint including the PDL-bone and PDL-cementum, endosteal bone-bone marrow [29], and blood vessel-fibrous periodontal ligament [3,6]. Strains can act in various forms and for a tissue like bone consisting of several channels through which dynamic fluid flow occurs, hoop strains could be dominant. Could this be the reason why there exists a concentric pattern around a blood vessel, and is it the hoop strain [30-35] in particular at the endosteal-bone marrow interface that prompts hematopoietic and/or stromal cells to differentiate into osteoblasts? Do osteoblasts lining along the inner endosteal wall generate layer-by-layer matrix inward? Although not presented within this manuscript, we often times see this occurring in bone (measured using the OPG/RANKL axis [36]) in various mammals including mice and rats, and could be the reason for secondary bone or osteonal bone formation [36,37] as seen in this study (Figs. 2c, 3 (stars indicating lower X-ray attenuation regions), 4, 5). Interestingly, a similar theory, but at a cellular level was proposed to illustrate that osteocytes within bone are mechanosensors as they continue to sense hoop strain and fluid shear within the perilacunar space, and put together they could maintain the quality of bone [31]. However, the sequence and orchestration of physical and chemical cues that prompt the bone lining cells to fabricate an organized matrix, let alone prompt biomineralization remains to be an ageless question.

It should be noted that within the strain induced secondary formations lies a distinct architecture that is dominated by collagen fibers. These are thought to be PDL-inserts [38] and are commonly within a uniformly spaced mineralized layer surrounding the tooth, called bundle bone, and clinically termed as the lamina dura due to its radiopacity [38]. In our study, the organic construct of the bony protrusion from the lamellar bone also contained a higher number of radial inserts, but fewer circumferential fibers, which made it structurally distinct from lamellar bone Figs. 2-5.

The presence of multiple architectures at the narrowed PDL-spaces; bundle bone, lamellar bone, inter-lamellae, and lamellae would make alveolar bone a heterogeneous tissue. However, of greater relevance to this work are the boundaries between lamellar and protruded bone that display steep or abrupt biochemical and/or mechanical changes (Figs. 2 - 8). We hypothesize, that the genesis of the observed interface between lamellar and protruded bone is due to a significant deviation from physiological strain. This interface not only exhibited a difference in tissue architecture, but illustrated an abundance of organic components at the protruded bone–lamellar bone junction (Figs. 3B & C, 6). The observed hygroscopicity can be correlated to the basophilic nature in hematoxylin and eosin sections of the complex (Fig. 2E & F) indicative of negatively-charged biomolecules. At the PDL-bone and PDL-cementum interfaces we identified both chondroitin and keratin-sulfated glycosaminoglycans, [39] which are contained within the small leucine rich proteoglycans, namely FMOD and BGN.

FMOD, an SLRP containing keratin-sulfated GAG with a fibrogenic potential is responsible for maintaining the integrity of organic matrices, and in our study was preserved in the organic-rich regions of bone and cementum (Fig. 4). However, BGN was observed at the PDL-bone attachment site and around the perilacunar space of osteocytes and sometimes

around cementocytes in other mammals [28]. Based on the localization of BGN, it is conceivable that osteoblastic to clastic activities are unbalanced in such a way to promote mineralization [28]. BGN influences osteoblast function through altering the activity of several growth factors including bone morphogenic proteins [40]. Additionally, BGN functions to regulate collagen fibrillogenesis, matrix structure, and biomineralization in specific tissues and maintains the periodontium during function [41-43]. BGN is thought to be released due to stress proteolytically from the extracellular matrix (ECM), and cleaved by enzymes including matrix metalloproteinases (MMPs) that can make it into a multivalent molecule [44]. The predominance of the multivalent molecule at the PDL-bone interface is of particular interest as it suggests a role as a potential chemical cue for secondary mineralization that could include abnormal growth of alveolar bone. Based on this data, it can be argued that the LB-protruded bone interface was the original site of PDL attachment, and that the growth leading to protrusions occurred as a result of shift in strain at the attachment site. Another indicator supporting this interpretation is the higher concentration of osteocytes at the junction indicating directional tissue growth (Fig. 3C). Should these secondary mineral formation events occur; basophilic lines are inevitable as they are also considered cement lines [38,45-47], which are dominant within protruded bone.

If mechanical load is the input signal at an organ level, strain modulated mineralization at a molecular scale is dependent on several factors. These factors include maturity of the organic matrix (including crosslink density), deposition of mineral within and around the collagen fibrils, and amorphous to crystalline transition of the mineral [48,49]. Parallel events include cell differentiation followed by maturity of mineral forming cells [30]. Hence, it can be argued that the secondary mineralization events need not exhibit the same physicochemical properties primary mineralized regions dominated by genetic inheritance.

The combination of these many events will undoubtedly make the tissue heterogeneous. In this study, we observed heterogeneity at several levels. Heterogeneity existed across lamellar and interlamellar regions, between lamellar bone and protruded bone, and within protruded bone itself. Interestingly, within lamellar bone and between lamellar bone and protruded bone, banding of hygroscopic regions was distinct. Correlating these hygroscopic regions to high resolution X-ray attenuation followed by electron transmission micrographs relayed interesting information. The hygroscopic regions were higher in X-ray attenuation compared to their interlamellar regions, and these regions contained crystalline minerals but also a dominance of collagen (Figs. 3, 5, 6). Within these regions were also identified elements such as Ca, Zn, and P, but the limitation was that we were unable to identify the spatial location of elements. In addition, the basophilic cement lines appeared as radiopaque lines (Figure 5), potentially due to the increased presence of Ca-based salts in these regions, as suggested by Weinmann [38]. It is also interesting to note that at the interface between bundle bone and lamellar bone, lamellae are all X-ray opaque, but demonstrated hygroscopic nature when scanned in wet using an AFM. This suggests that the collagen fibrils contain intrafibrillar crystalline mineral giving them the necessary elasticity to prevent nonlinear deformation from radial strains by fluid pressure within the tissue, and pullout forces at the PDL-bone and PDL-cementum interfaces. This can be further argued that tissues loaded in compression exhibit significant extrafibrillar mineral. Additionally, it was illustrated that secondary bone consists of a greater amount of cementing substance than

regular lamellar bone, rendering the tissue more radiopaque [38]. Hence, it is possible that the cementing elements contribute to a higher opacity within collagen fiber dense lamellae, and protruded bone.

In this study, at bony protrusion site, higher concentrations of Ca, P including the presence of Zn can only be warranted for the patient's age from which bone was extracted. Secondary bone formation can also be regulated by hormone, vitamin, and ion presence within the patient [50,51]. While Ca and P contents can change, of particular interest is the localization of zinc within specific sites. Zinc is a molecule believed to be associated with function- and disease-induced biomineralization both of which require different levels of tissue turnover. Zinc is necessary for matrix metalloproteases to be activated and furthermore to note is that certain proteases require mechanical strain to be docked with Zn in order to become functionally active. Additionally, various zinc finger proteins have been shown to be directly or indirectly related to the regulation of osteoblast differentiation and thereby bone formation via levels of Runx2, the principal transcriptional regulator of osteoblast differentiation [52,53]. In fact, for the Osx zinc finger protein, Osx null mice demonstrated no ossification [54]. Zinc has also been shown to play a role in bone volume density, where age related stages of bone maturation could be affected by increasing Zn [55]. Interestingly, Zn was localized in bundle bone, suggesting bundle bone may be associated with an early adaptive response of the bone-PDL-tooth complex. As a result, increased site specific resistance to mechanical loads was observed in bundle bone compared to lamellar bone.

Given the structural and chemical heterogeneity within the tissue we did not identify bundle bone or lamellar bone with a constant value for E_r. Rather, they were related to a range for heterogeneous lamellar bone, and bundle bone respectively. However, the higher range for bundle bone when compared to lamellar could be due to rate and frequency dependence of input stimuli. Frequency and magnitude can prompt different response from mineral forming and resorbing cells. Hence, from a functional perspective, do these protrusion in bone with a higher elastic modulus, higher levels of Ca, P, and Zn, despite their dominance in hygroscopic radial fibers cause an elastic discontinuity in bone, and does this discontinuity within the tissue and in the joint *per se* [6] shift physiological to maladapted function or pathology?

Just considering bone, current literature illustrates a number of descriptors for normal or physiological state of bone. Factors include the cellular origin of bone, degree of mineralization or remodeling, physicochemical heterogeneity, resistance to fracture, and from the results of this study, an emergence of an elastic discontinuity. Most often the state of bone is identified by an overarching term, i.e. "quality" to describe its functional ability. It is important to note that the leading American Society for Bone Mineral Research (ASBMR) lecture series, identified bone quality as the "turnover, damage accumulation (e.g. microfractures) and mineralization of the organic matrix, the chemical composition and extent of crosslinking of the organic matrix, bone architecture, fatigue from repeated loading of bone, the rate and direction of deformation of the bone during trauma and is determined by a complex interplay between the amount of mineralized tissue present in the bone, and the extent of biomineralization" [56]. Given this broad spectrum of properties that could be incorporated into "quality", it is clear that this heterogeneous and dynamic tissue that plays

such an important role in tooth function cannot be simply described by a sole parameter. The goal of this argument is not to introduce a newer definition to “bone quality”. It is to provide an insight as to whether or not adaptations in bone maintain optimum function or does it shift the structure to a maladapted state leading to pathology to address functional demands on the organ. By linking biological factors to physicochemical results, the concept of bone quality is one step closer to becoming a quantifiable property.

Within the organ, alveolar bone along with its protrusions works in concert with other tissue, one of which is cementum. Cementum is an essential part of the tooth complex as it aids in tooth attachment to alveolar bone. Additionally, it is necessary to point the architectural similarities between cementum and that of bony protrusions, in that both tissues are dominated by radial fibers. Most often it is thought that cementum is lamellar, does not adapt, or has minimal adaptive response. While this could be true when compared to vascularized bone, based on results presented in Fig. 2, it is plausible that cementum, although perhaps not reactive at the same rate as vascularized bone, could have a delayed response. If so, could this be the reason why bone grows into the PDL-space, while cementum subsequently makes way to accommodate the growth? And could this be the reason why secondary events such as conforming or nonconforming forms of cementum occur?

The results of this study highlight two points: 1. the genesis of protrusions and 2. the role of protruded bone on the overall quality of alveolar bone *per se*, during function of the bone-PDL-tooth fibrous joint. From careful consideration of the results the bony protrusions are mineralized tissues generated at the mechanically strained periodontal ligament closer to bone. To explain the aforementioned phenomena we present a model representing local fluctuations in mechanical strain that could explain adaptation of bone resulting in heterogeneous properties of individual tissues that form the complex. The proposed model in Fig. 9 is an extrapolation of fundamentals from orthopedics that states that the anatomical axis and loading axis should coincide for physiological function of a joint (Fig. 9 A). Zones Z1, and Z3 (with stiffness values of S1-S3) represent strains within the differentiating zones at the PDL-bone, and PDL-cementum sites *per se*, while Z2 represents stiffness of the fibroblastic PDL. It was reported that Z1 and Z3 are strain amplification sites owing to the attachment of a dissimilar softer tissue with a harder tissue [57] with different stiffness values. However, if eccentric loading perpetuates, joint impairment is inevitable (Fig. 9B & C). as it promotes uneven strain fields within the complex let alone the entire joint, i.e. bone-PDL-tooth fibrous joint. A shift in mechanical strain can prompt increased pullout forces at the PDL-bone attachment sites (Z1) causing cells to differentiate and undergo different rates of durotaxis and haptotaxis. Perpetuating loading can shift an original tension based zone to a compression zone at Z3 (Fig. 9B). The increased compression in Z3 can cause cementum resorption in an attempt to maintain necessary PDL-space. It should be noted that the faster bone turnover rate and slower response of cementum to mechanical strain explains the observed events in this study. The resulting distinct difference between bundle bone and lamellar bone raises the question on the overall quality of bone from a functional perspective.

5. CONCLUSION

In this study, narrowed PDL-spaces in the bone-PDL-tooth fibrous joint were investigated with high resolution structural, biochemical and mechanical techniques. The dissimilarity of tissues at the attachment sites within the complex, namely the chemical heterogeneity and elastic mismatch between lamellar bone, bundle bone, PDL and cementum, presents itself as strain amplification sites. The genesis of bundle bone and adapted cementum at the original ligament-bone and ligament-cementum attachment arise to resist the combinatorial force field during function. These semiautonomous events lead us to propose that the natural plasticity of the bone-PDL-tooth fibrous joint continues to guide the organ within physiological limits, but significant mineral formation or resorption related events may result in closing or widening of the PDL-space and can guide the complex to a nonphysiological regime.

Supplementary Material

Refer to Web version on PubMed Central for supplementary material.

Acknowledgments

The authors acknowledge funding support NIH/NIDCR R00DE018212 (SPH), NIH/NIDCR-R01DE022032 (SPH), NIH/NIDCR T32 DE07306, NIH/NCRR S10RR026645, (SPH) and Departments of Preventive and Restorative Dental Sciences and Orofacial Sciences, UCSF; Faculty of Engineering, McMaster University (Hamilton, Canada) (KG). In addition, assistance from national facilities through user based program was provided by Stanford Synchrotron Radiation Lightsource (SSRL), SLAC National Accelerator Laboratory, Stanford University, CA and The Molecular Foundry, Lawrence Berkeley National Laboratory, Berkeley, CA. The TXM work performed at SSRL, SLAC was done on TXM purchased through a grant from National Institutes of Health (NIH)/National Institute of Biomedical Imaging and Bioengineering grant number R01-EB004321 (PP). Work at the SSRL was supported by the U.S. Department of Energy under contract number DE-AC02-76SF00515. Work at the Molecular Foundry was supported by the Office of Science, Office of Basic Energy Sciences, of the U.S. Department of Energy under Contract No. DE-AC02-05CH11231.

References

1. Nanci, A. Ten Cate’s Oral Histology. Mosby Elsevier; St. Louis: 2008.
2. van den Bos T, Beertsen W. Alkaline phosphatase activity in human periodontal ligament: age effect and relation to cementum growth rate. J Periodontal Res. 1999; 34:1–6. [PubMed: 10086880]
3. Ho SP, Kurylo MP, Fong TK, Lee SSJ, Wagner HD, Ryder MI, et al. The biomechanical characteristics of the bone-periodontal ligament-cementum complex. Biomaterials. 2010; 31:6635–6646. [PubMed: 20541802]
4. Thompson, DW. On Growth and Form. Cambridge University Press; 1961. On form and mechanical efficiency; p. 221
5. Wolff, J. The law of bone remodelling. Springer Verlag; Berlin: 1986.
6. Hurng JM, Kurylo MP, Marshall GW, Webb SM, Ryder MI, Ho SP. Discontinuities in the human bone-PDL-cementum complex. Biomaterials. 2011; 32:7106–7117. [PubMed: 21774982]
7. Benjamin M, Kumai T, Milz S, Boszczyk BM, Boszczyk AA, Ralphs JR. The skeletal attachment of tendons--tendon “entheses”. Comp Biochem Physiol Part a Mol Integr Physiol. 2002; 133:931–945.
8. Benjamin M, McGonagle D. Entheses: tendon and ligament attachment sites. Scandinavian Journal of Medicine & Science in Sports. 2009; 19:520–527. [PubMed: 19522749]
9. Benjamin M, Moriggl B, Brenner E, Emery P, McGonagle D, Redman S. The “enthesis organ” concept: Why enthesopathies may not present as focal insertional disorders. Arthritis Rheum. 2004; 50:3306–3313. [PubMed: 15476254]

10. Benjamin M, Ralphs JR. Entheses--the bony attachments of tendons and ligaments. Italian J Anat Embryol. 2001; 106:151–157.
11. Benjamin M, Ralphs JR. Fibrocartilage in tendons and ligaments - an adaptation to compressive load. J Anatomy. 1998; 193:481–494.
12. Benjamin M, Ralphs JR. Tendons and ligaments-an overview. Histology and Histopathology. 1997; 12:1135–1144. [PubMed: 9302572]
13. Brauer DS, Saeki K, Hilton JF, Marshall GW, Marshall SJ. Effect of sterilization by gamma radiation on nano-mechanical properties of teeth. Dent Mater. 2008; 24:1137–1140. [PubMed: 18436298]
14. Ten Cate, AR. Oral histology. 5. Mosby Inc; 1998.
15. Ho SP, Goodis H, Balooch M, Nonomura G, Marshall SJ, Marshall G. The effect of sample preparation technique on determination of structure and nanomechanical properties of human cementum hard tissue. Biomaterials. 2004; 25:4847–4857. [PubMed: 15120532]
16. Ho SP, Balooch M, Goodis HE, Marshall GW, Marshall SJ. Ultrastructure and nanomechanical properties of cementum dentin junction. J Biomed Mater Res. 2004; 68:343–351.
17. Balooch G, Marshall GW, Marshall SJ, Warren OL, Asif SAS, Balooch M. Evaluation of a new modulus mapping technique to investigate microstructural features of human teeth. J Biomech. 2004; 37:1223–1232. [PubMed: 15212928]
18. Ho SP, Senkyrikova P, Marshall GW, Yun W, Wang Y, Karan K, et al. Structure, chemical composition and mechanical properties of coronal cementum in human deciduous molars. Dent Mater. 2009; 25:1195–1204. [PubMed: 19464049]
19. Marshall GW, Balooch M, Gallagher RR, Gansky SA, Marshall SJ. Mechanical properties of the dentinoenamel junction: AFM studies of nanohardness, elastic modulus, and fracture. J Biomed Mater Res. 2001; 54:87–95. [PubMed: 11077406]
20. Ho SP, Balooch M, Marshall SJ, Marshall GW. Local properties of a functionally graded interphase between cementum and dentin. J Biomed Mater Res. 2004; 70:480–489.
21. Andrews JC, Almeida E, van der Meulen MCH, Alwood JS, Lee C, Liu Y, et al. Nanoscale X-ray microscopic imaging of mammalian mineralized tissue. Microsc Microanal. 2010; 16:327–336. [PubMed: 20374681]
22. Grandfield K, Palmquist A, Engqvist H. High-resolution three-dimensional probes of biomaterials and their interfaces. Philos T R Soc A. 2012; 370:1337–1351.
23. Lin JD, Özcoban H, Greene JP, Jang AT, Djomehri SI, Fahey KP, et al. Biomechanics of a bone–periodontal ligament–tooth fibrous joint. J Biomech. 2013; 46:443–449. [PubMed: 23219279]
24. Herring, SW. Biomechanics of teeth in bone: function, movement and prosthetic rehabilitation. In: McCauley, LK.; Somerman, MJ., editors. Mineralized Tissues in Oral and Craniofacial Science: Biological Principles and Clinical Correlates. John Wiley & Sons, Inc; 2012.
25. Weinmann JP. Bone Changes Related to Eruption of the Teeth*. The Angle Orthodontist. 1941; 11:83–99.
26. Herber R-P, Fong J, Lucas SA, Ho SP. Imaging an Adapted Dentoalveolar Complex. Anatomy Research International. 2012; 2012:1–13.
27. Leong NL, Hurng JM, Djomehri SI, Gansky SA, Ryder MI, Ho SP. Age-Related Adaptation of Bone-PDL-Tooth Complex: Rattus-Norvegicus as a Model System. PLoS ONE. 2012; 7:e35980. [PubMed: 22558292]
28. Chiu R, Li W, Herber RP, Marshall SJ, Young M, Ho SP. Effects of biglycan on physico-chemical properties of ligament-mineralized tissue attachment sites. Archives of Oral Biology. 2012; 57:177–187. [PubMed: 21963335]
29. Kristensen HB, Andersen TL, Marcussen N, Rolighed L, Delaisse J-M. Increased presence of capillaries next to remodeling sites in adult human cancellous bone. J Bone Miner Res. 2013; 28:574–585. [PubMed: 22991221]
30. Bonewald LF. Mechanosensation and Transduction in Osteocytes. Bonekey Osteovision. 2006; 3:7–15. [PubMed: 17415409]
31. Bonewald LF. The amazing osteocyte. J Bone Miner Res. 2011; 26:229–238. [PubMed: 21254230]

32. Han YF, Cowin SC, Schaffler MB, Weinbaum S. Mechanotransduction and strain amplification in osteocyte cell processes. Proc Natl Acad Sci USA. 2004; 101:16689–16694. [PubMed: 15539460]
33. Kamioka H, Yamashiro T. Mechanosensitivity of osteocytes. Clin Calcium. 2012; 22:697–704. [PubMed: 22549194]
34. Kamioka H, Yamashiro T. Osteocytes and mechanical stress. Clin Calcium. 2008; 18:1287–1293. [PubMed: 18758034]
35. Bonewald LF. Your bone cells are watching you. The American Society for Bone and Mineral Research. 2013
36. Robling AG, Castillo AB, Turner CH. Biomechanical and molecular regulation of bone remodeling. Annu Rev Biomed Eng. 2006; 8:455–498. [PubMed: 16834564]
37. Roberts WE, Roberts JA, Epker BN, Burr DB, Hartsfield JK Jr. Remodeling of Mineralized Tissues, Part I: The Frost Legacy. Seminars in Orthodontics. 2006; 12:216–237.
38. Weinmann, JP.; Sicher, H. Bone and bones. The C.V. Mosby Company; St. Louis: 1955.
39. Kurylo, MP.; Nonomura, G.; Marshall, GW.; Schuck, PJ.; Ho, SP. Localization and Physico-chemical Effects of Glycosaminoglycans within Molar Interfaces. 89th General Session and Exhibition of the IADR; San Diego, CA, USA. 2011.
40. Young MF, Bi YM, Ameye L, Chen XD. Biglycan knockout mice: New models for musculoskeletal diseases. Glycoconj J. 2002; 19:257–262. [PubMed: 12975603]
41. Tenório DMH, Santos MF, Zorn TMT. Distribution of biglycan and decorin in rat dental tissue. Braz J Med Biol Res. 2003; 36:1061–1065. [PubMed: 12886460]
42. Matheson S, Larjava H, Hakkinen L. Distinctive localization and function for lumican. fibromodulin and decorin to regulate collagen fibril organization in periodontal tissues. J Periodontal Res. 2005; 40:312–324. [PubMed: 15966909]
43. Kalamajski S, Oldberg A. The role of small leucine-rich proteoglycans in collagen fibrillogenesis. Matrix Biol. 2010; 29:248–253. [PubMed: 20080181]
44. Nastase MV, Young MF, Schaefer L. Biglycan: A Multivalent Proteoglycan Providing Structure and Signals. J Histochem Cytochem. 2012; 60:963–975. [PubMed: 22821552]
45. Burr DB, Schaffler MB, Frederickson RG. Composition of the cement line and its possible mechanical role as a local interface in human compact bone. J Biomech. 1988; 21:939–945. [PubMed: 3253280]
46. Seeman E, Delmas PD. Bone quality--the material and structural basis of bone strength and fragility. N Engl J Med. 2006; 354:2250–2261. [PubMed: 16723616]
47. Carter, DR.; Beaupré, GS.; Beaupré, GS. Skeletal Function and Form. Cambridge University Press; Cambridge: 2001.
48. Termine JD, Posner AS. Infrared Analysis of Rat Bone: Age Dependency of Amorphous and Crystalline Mineral Fractions. Science. 1966; 153:1523–1525. [PubMed: 5917783]
49. Blumenthal NC, Betts F, Posner AS. Effect of Carbonate and Biological Macromolecules on Formation and Properties of Hydroxyapatite. Calcif Tissue Res. 1975; 18:81–90. [PubMed: 1148899]
50. Raisz LG, Bingham PJ. Effect of hormones on bone development. Annu Rev Pharmacol. 1972; 12:337–352. [PubMed: 4339020]
51. Ramfjord SP, Blankenship JR. Increased occlusal vertical dimension in adult monkeys. J Prosthet Dent. 1981; 45:74–83. [PubMed: 7007628]
52. Hesse E, Kiviranta R, Wu M, Saito H, Yamana K, Correa D, et al. Zinc finger protein 521, a new player in bone formation. Ann N Y Acad Sci. 2010; 1192:32–37. [PubMed: 20392215]
53. Jones DC. Regulation of Adult Bone Mass by the Zinc Finger Adapter Protein Schnurri-3. Science. 2006; 312:1223–1227. [PubMed: 16728642]
54. Nakashima K, Zhou X, Kunkel G, Zhang Z, Deng JM, Behringer RR, et al. The novel zinc finger-containing transcription factor osterix is required for osteoblast differentiation and bone formation. Cell. 2002; 108:17–29. [PubMed: 11792318]
55. Laudermilk MJ, Manore MM, Thomson CA, Houtkooper LB, Farr JN, Going SB. Vitamin C and Zinc Intakes are Related to Bone Macroarchitectural Structure and Strength in Prepubescent Girls. Calcified Tissue International. 2012; 91:430–439. [PubMed: 23076447]

56. Parfitt AM, Goldstein S, Compston J. Bone Quality: What is it and can we measure it? The American Society for Bone and Mineral Research. 2005

57. Qian L, Todo M, Morita Y, Matsushita Y, Koyano K. Deformation analysis of the periodontium considering the viscoelasticity of the periodontal ligament. Dent Mater. 2009; 25:1285–1292. [PubMed: 19560807]

HIGHLIGHTS

- An adapted human bone-periodontal ligament (PDL)-tooth fibrous joint was highlighted by a narrowed PDL-space and presence of adapted bone.
- Bony protrusion(s) or adaptations identified as bundle bone with structural, biochemical, and mechanical heterogeneities, was dissimilar from lamellar bone.
- The observed physicochemical heterogeneities could be the functional cues for an original PDL-bone to serve as the genesis for bony protrusions.
- Heterogeneous constructs contained physicochemical discontinuities in the bone-PDL-tooth fibrous joint could be “markers” indicative of pathological adaptation of alveolar bone.
- Bony adaptations or protrusions within the complex can perpetuate functional demands and shift the organ to a pathological regime.

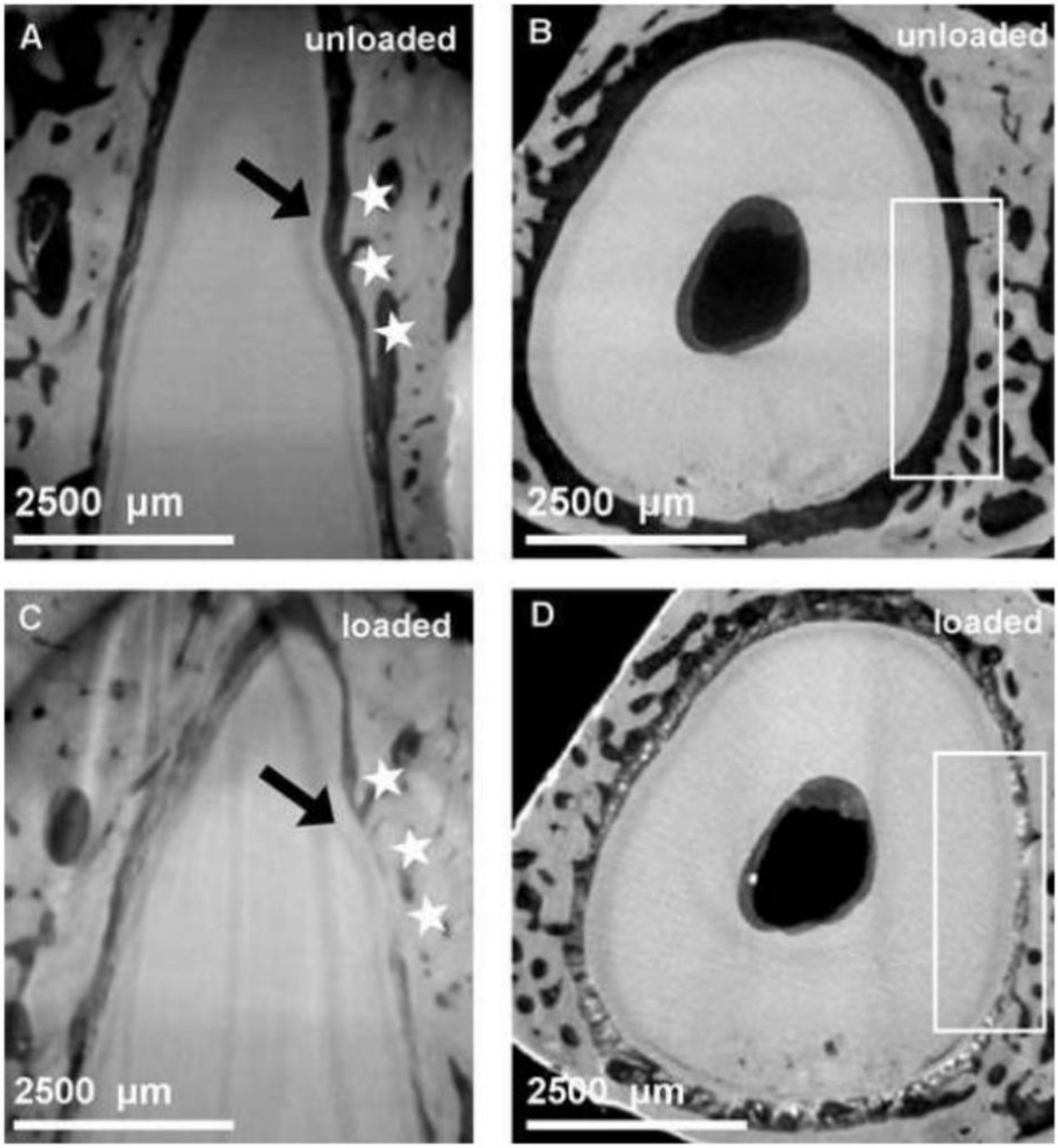

Figure 1. Qualitative assessment of conforming and nonconforming bone-tooth root surfaces at no load (TOP row) and loaded (BOTTOM row) conditions

Seemingly conforming surfaces are illustrated in an unloaded bone-PDL-tooth complex **(A, B)** stained with phosphotungstic acid (PTA) [3]. However, under loaded conditions the non-conforming tooth root and alveolar bone surface sites (white stars and box) are highlighted **(C, D)**.

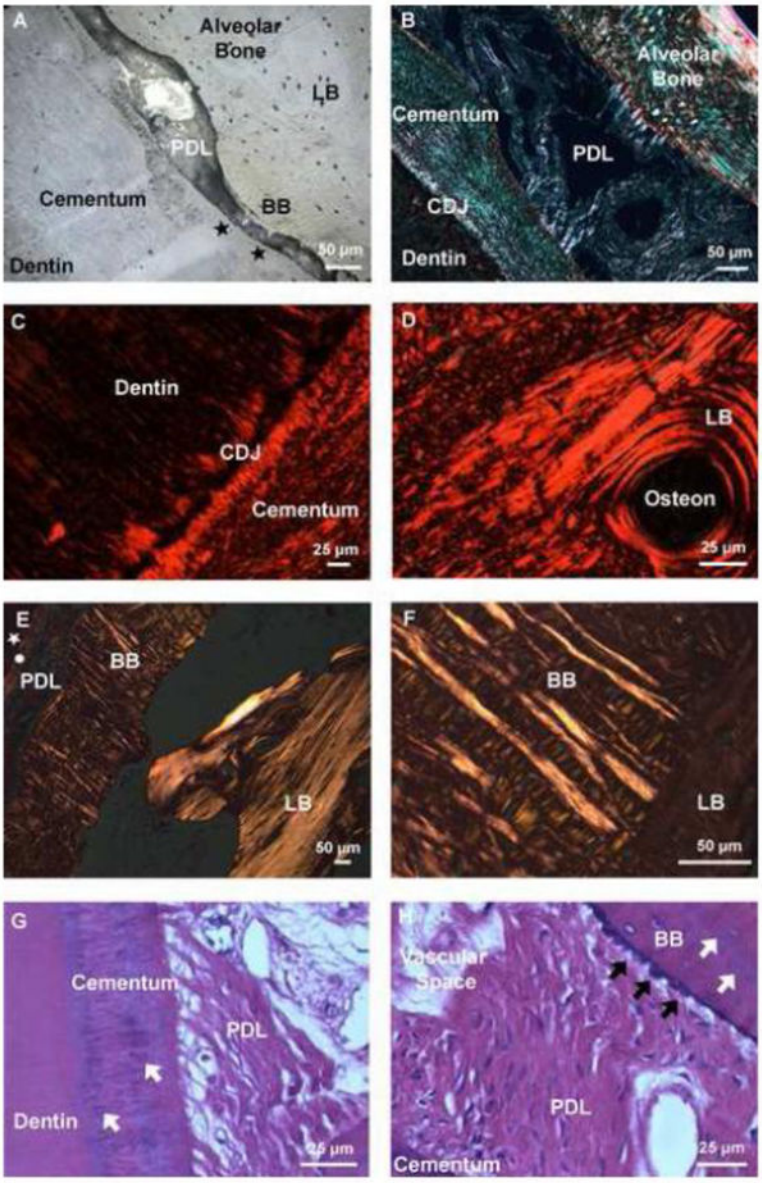

Figure 2. Fiber orientation varied across tissues of the bone-PDL-cementum complex

Higher magnification light micrograph of an ultrasectioned surface block illustrated structural heterogeneity in alveolar bone, PDL, and tooth. The tissue-level characteristics of constricted PDL-space include invasion of BB from LB and adapted cementum (black stars) **(A)**. Picrosirius red stain coupled with polarized light microscopy of the narrowed region demonstrated differential fiber orientation within secondary cementum and alveolar bone **(B)**, and the differential collagen fiber orientation between the cementum dentin junction (CDJ), and lamellae and interlamellae regions (characterized by birefringence) **(C, D)**. Lower and higher magnification hematoxylin and eosin staining (H&E) of alveolar bone coupled with polarized light microscopy demonstrated the heterogeneity of fiber orientation between BB, which was dominated by radial fibers, versus LB consisting of primarily circumferential fibers (circle: cementum, white star: dentin) **(E,F)**. Hematoxylin and eosin

staining (H&E) demonstrated localization of basophilic lines in both cementum and bundle bone (white arrows). Additionally, directional bone growth illustrated by bony protrusions (black arrows) was expressed at the PDL-bone interface **(G,H)**. LB: Lamellar bone, BB: Bundle bone, PDL: Periodontal ligament, CDJ: Cementum-dentin junction. *Note: the orientation of the bone-PDL-tooth complex varies in images.

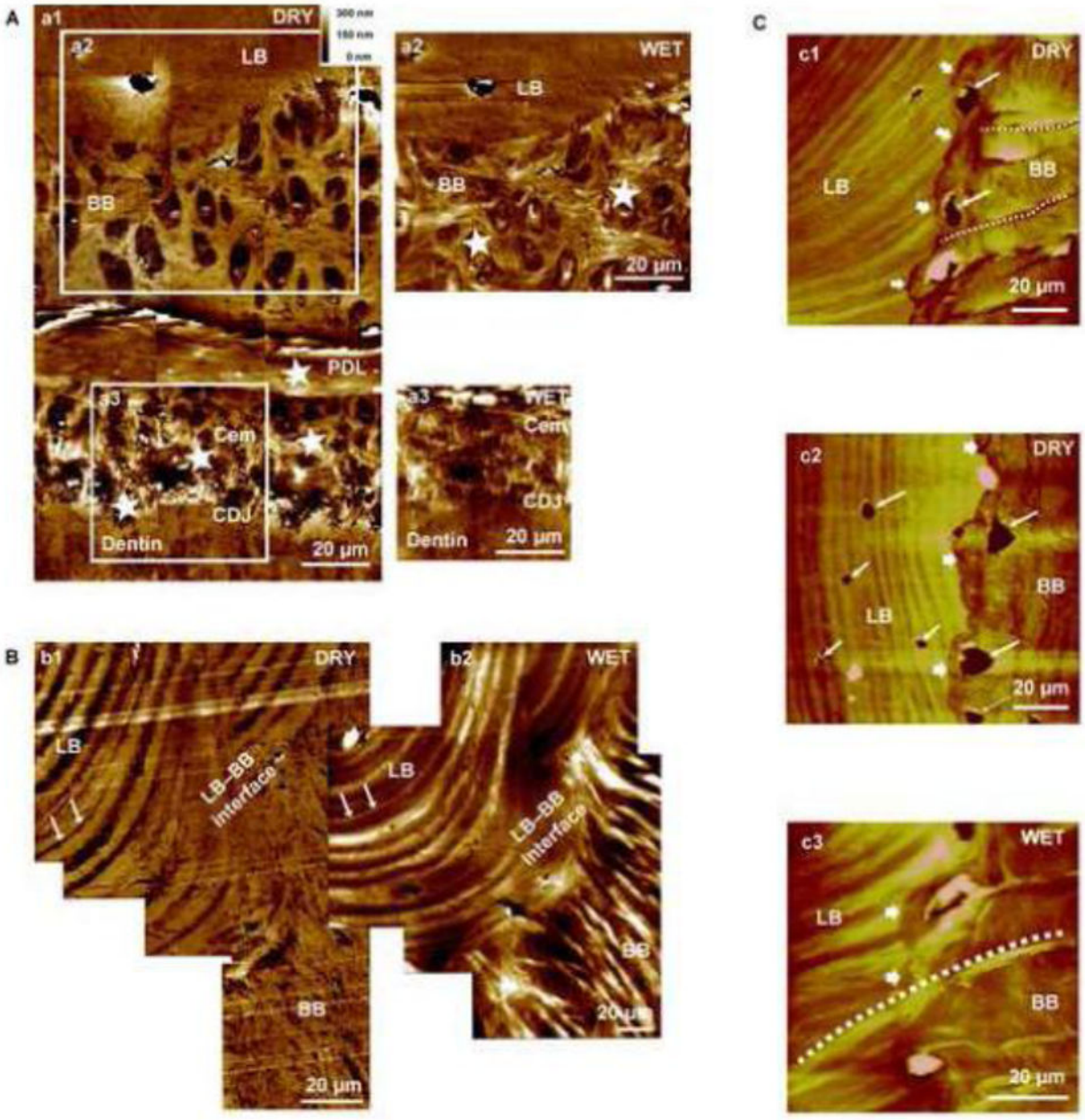

Figure 3. Tissue architecture under dry and wet conditions illustrated LB-BB interface as the original site of PDL attachment

Higher resolution AFM micrograph of an alveolar bone-PDL-cementum complex imaged under dry **(A: a1)** and wet **(A: a2, a3)** conditions. Radial fiber insertions (stars, cross sections revealed) into both BB and cementum interfacing the PDL are visible. Swelling of insertion fibers (stars) under wet conditions are indicative of polyanionic molecules and predominance of organic matter. The LB-BB interface is shown in greater detail under dry **(B: b1)** and wet **(B: b2)** conditions. Under dry conditions, lamellae regions demonstrated greater depth relative to inter-lamellae regions of LB. However, under wet conditions lamellae regions demonstrated increased hygroscopicity compared to inter-lamellae regions of LB, suggestive of differential degrees of mineral and/or organic content. A corresponding

lamellar region is denoted by arrows in both dry and wet conditions. It should be a noted that angle of sectioning can illustrate a structure significantly different from the LB-BB interface, as observed in B: b2. Additionally, continuous fibers from BB through the distinct interface and attached to LB are visible **(C: c1, c2, c3)**. All images exhibited hygroscopicity under wet conditions **(C: c3)** and insertion of Sharpey's fibers across BB and into the LB region, alongside multiple osteocytes, indicates the LB–BB interface as the point of genesis for BB growth. LB: Lamellar bone, BB: Bundle bone, PDL: Periodontal ligament, Cem: Cementum, CDJ: Cementum-Dentin Junction.

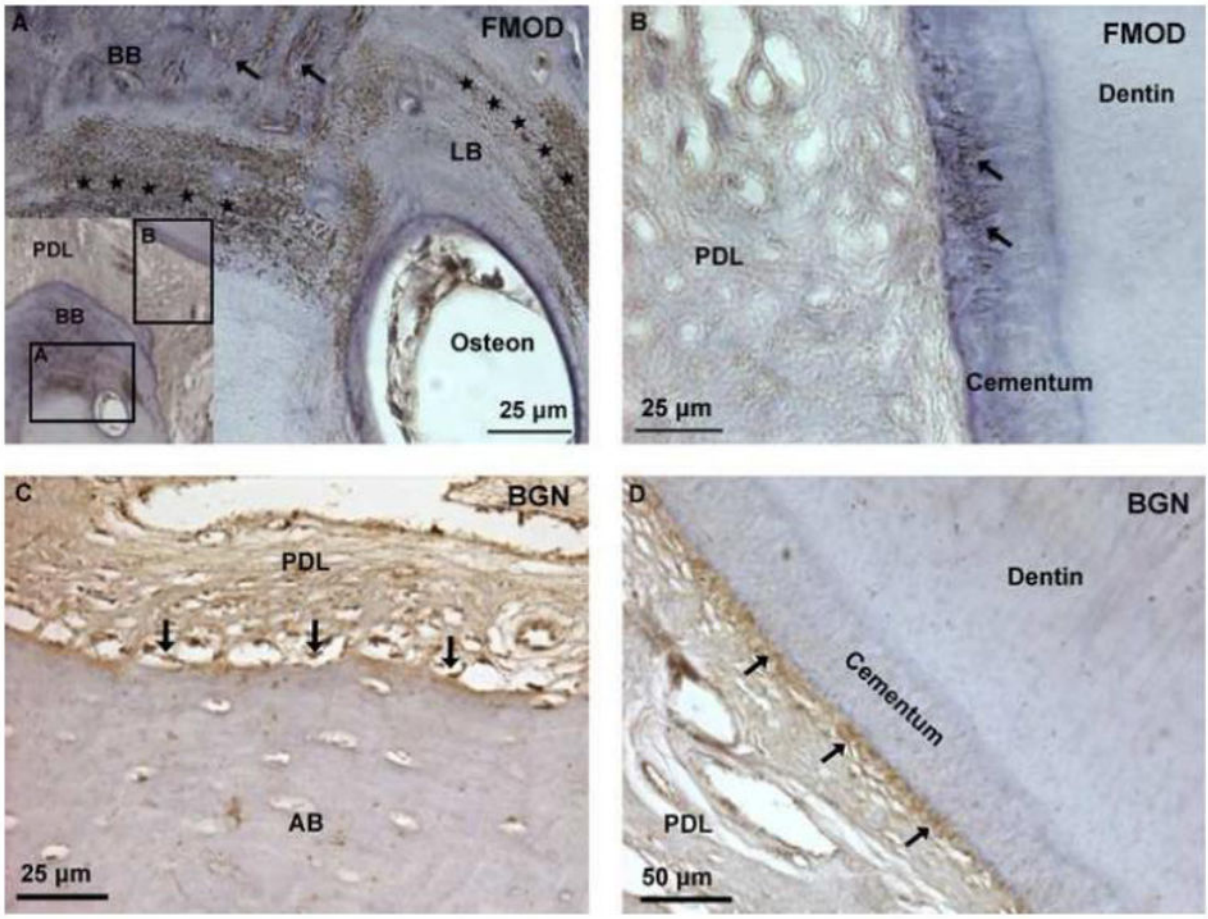

Figure 4. Presence of fibromodulin and biglycan small leucine rich proteoglycans at the PDL-bone and PDL-cementum interfaces

Immunohistochemistry identified localized fibromodulin (FMOD) in Sharpey's fibers of cementum and BB (arrows), and within interlamellae and lamellae regions of LB (stars) **(A, B)**. Expression of biglycan (BGN) was localized at the PDL-cementum and PDL-alveolar bone interfaces (arrows) **(C, D)**.

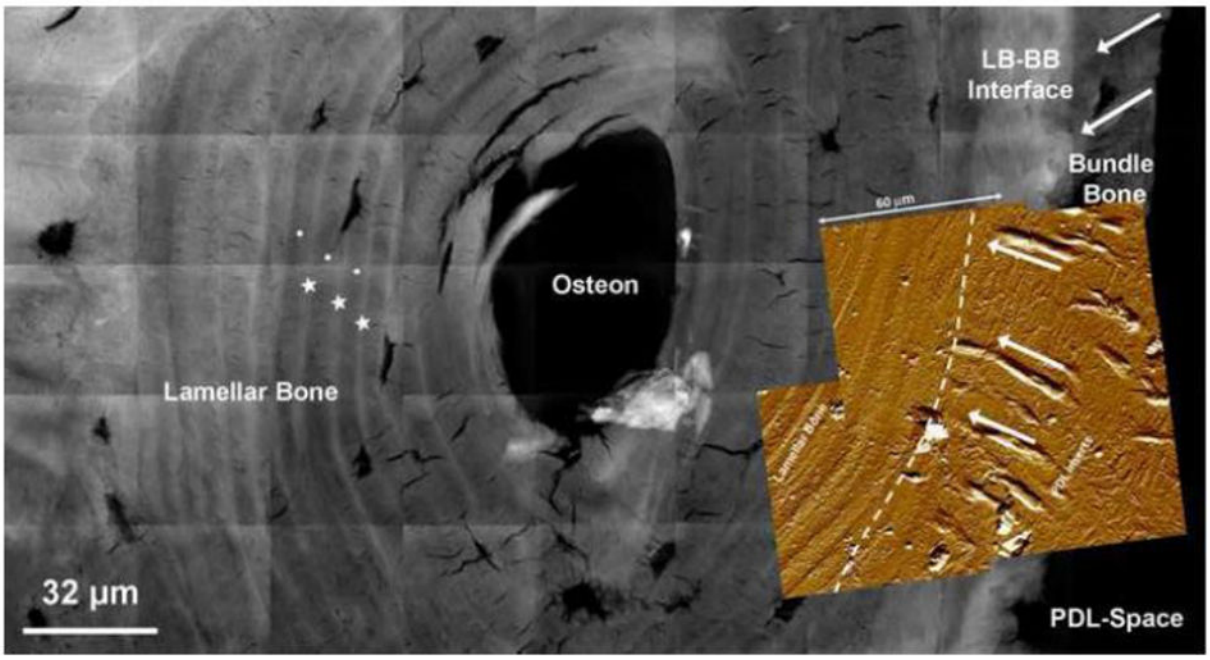

Figure 5. A higher resolution map of heterogeneous X-ray attenuations within alveolar bone

A composite made out of micrographs taken using a high resolution Nano-TXM illustrated varying X-ray attenuations within bundle bone (BB). Bone adjacent to the PDL-space was identified as BB by the presence of less attenuating organic Sharpey's fibers inserts (white arrows). Interestingly, the LB-BB interface is highlighted as highly X-ray attenuating suggesting higher mineral content. Overlay is an AFM micrograph with radial PDL fibers in BB and an orientation change to circumferential in LB within a junction of 10-30 µm. It is possible that the density of fibers could have contributed to the higher X-ray attenuation (dashed white line). Highly attenuated (radiopaque) regions (star) in lamellar bone (circle). Lamellar bone: LB, Bundle bone: BB, Periodontal ligament: PDL

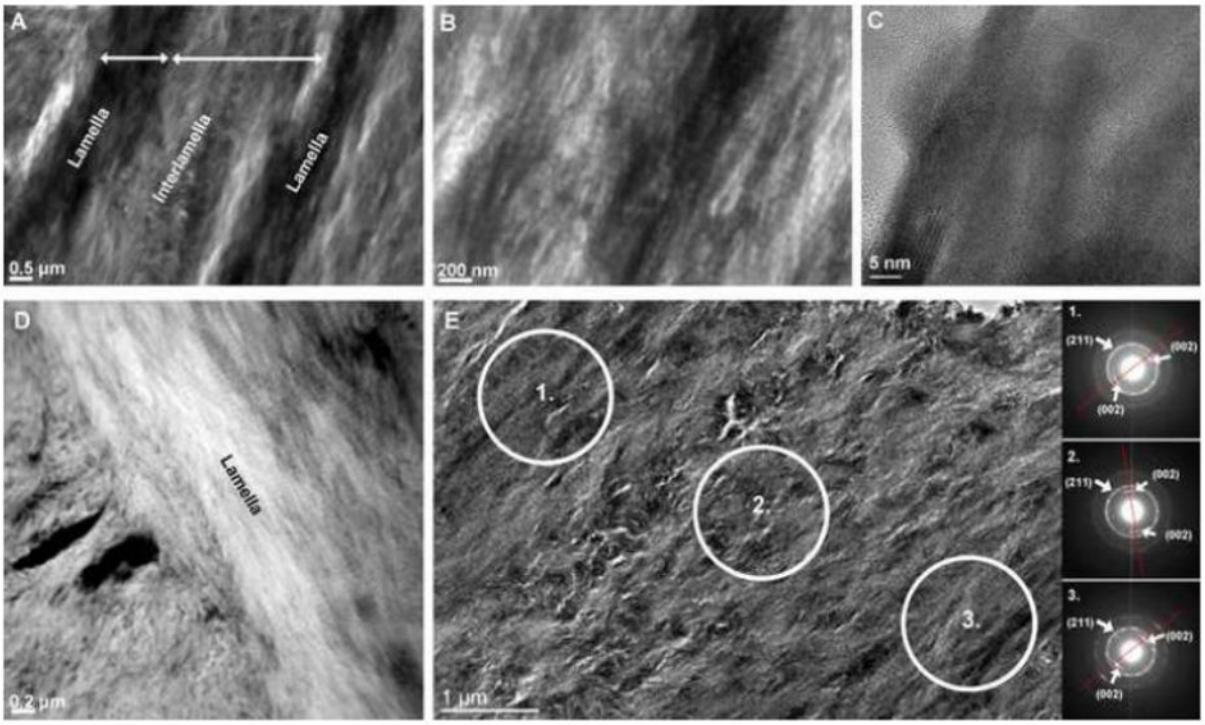

Figure 6. Complementary TEM data illustrated electron dense lamellar regions with visible collagen and possibly intrafibrillar mineral

Conventional TEM micrographs illustrate interlamellae and lamellae regions of lamellar bone **(A)** with visible collagen banding **(B)** and high resolution lattice fringes confirm crystallinity of the apatite mineral phase **(C)**. High angle annular dark field STEM images **(D)** give rise to a slight compositional contrast of lamella and interlamellae regions. Selected area diffraction patterns **(E)** also highlight the varying and preferred texture of crystals within these regions. The preferred orientation of the c-axis of the crystal, corresponding to the (002) direction, is indicated by red lines on the diffraction pattern.

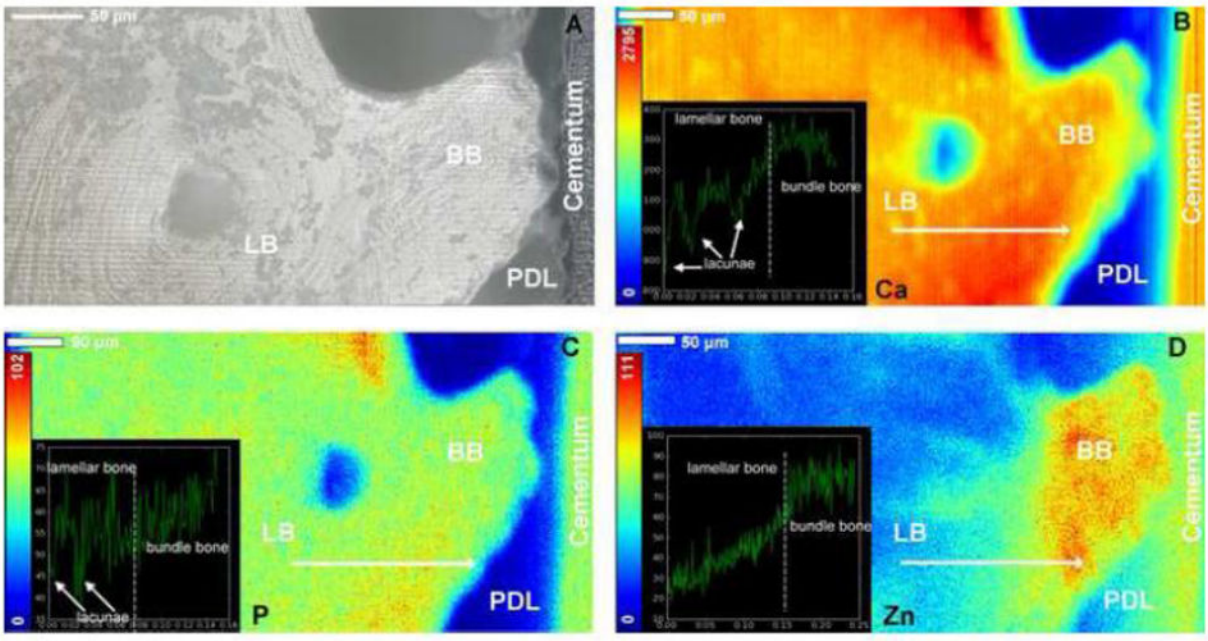

Figure 7. Presence of higher amounts of Zn and Ca in bony protrusions

Light micrograph of bony protrusion identified as bundle bone, protruding into the PDL-space towards cementum of the tooth **(A)**. High resolution micro-XRF spatial maps of elemental Calcium (Ca) **(B)**, Phosphorus (P) **(C)**, and Zinc (Zn) **(D)** demonstrated higher X-ray fluorescence counts of Ca and P in BB relative to LB. Corresponding line maps (overlays) illustrated steep gradients in Ca and P at the LB-BB interface. Additionally, several lacunae in alveolar bone were identified (white arrows). Interestingly, a distinct localization of Zn, an element theorized as a potential marker for function- and disease-induced biomineralization was observed in BB and cementum. Lamellar bone: LB, Bundle bone: BB

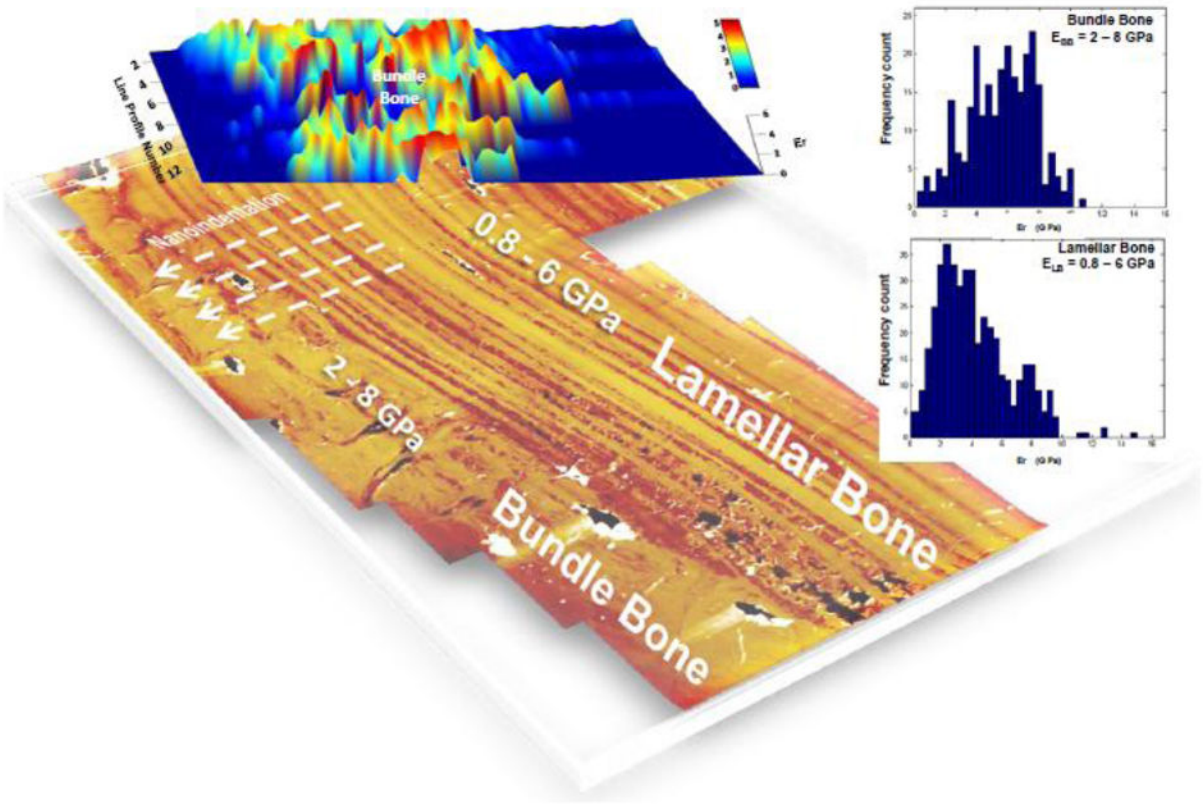

Figure 8. Heterogeneity in elastic modulus within and across bundle bone and lamellar bone

Three-dimensional plot of reduced elastic modulus (Er) overlaid on an AFM image illustrating the location of site-specific nanoindentation measurements. As illustrated via frequency plots, bundle bone demonstrated higher reduced elastic modulus values ranging from 2-8 GPa compared to 0.8-6 GPa for lamellar bone. All values are from hydrated tissues. LB: Lamellar bone, BB: Bundle bone

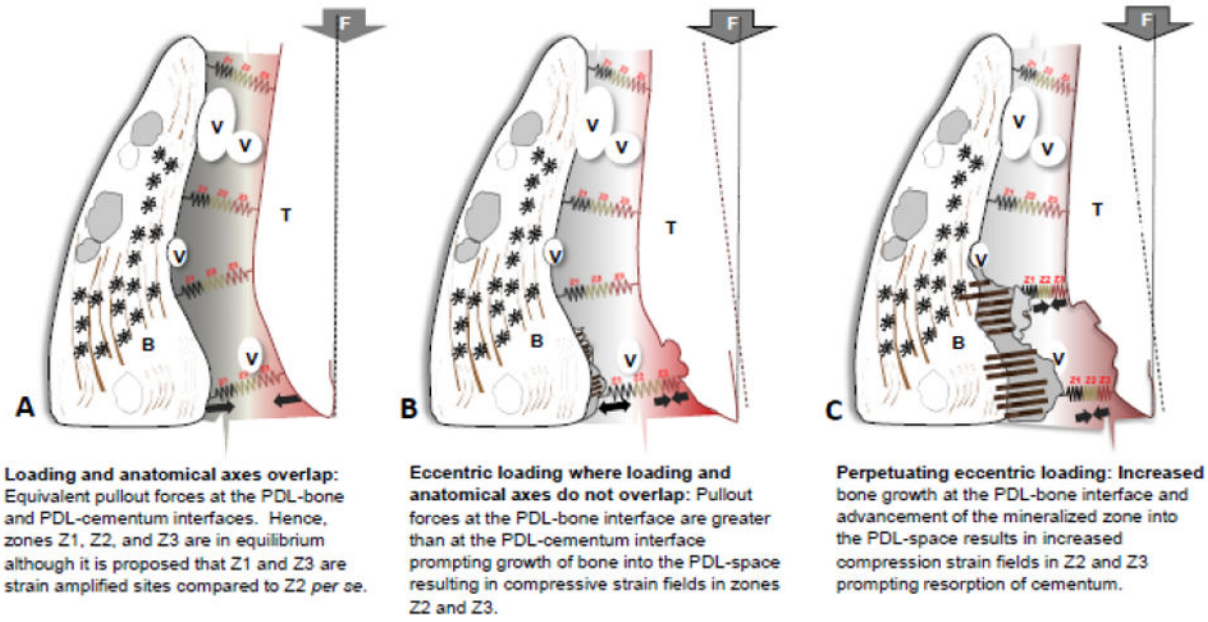

Figure 9. A biomechanical model postulating events that led to observed results

Results presented within the manuscript provided us insights to develop the following model. The model represents local fluctuations in mechanical strain that could explain adaptation of bone resulting in heterogeneous properties of individual tissues that form the compromised tooth-PDL-bone complex. Zones Z1, Z2, and Z3 represent strains at the PDL-bone, PDL per se, and PDL-cementum sites. It was documented that Z1 and Z3 are strain amplification sites owing to the attachment of a dissimilar softer tissue with a harder tissue (Qian et al.). The proposed model is an extrapolation of fundamentals from orthopedics that states that the anatomical axis and loading axis should coincide for physiological function of a joint **(A)**. However, if eccentric loading perpetuates, joint impairment is inevitable **(B, C)**, because it promotes uneven strain fields and increased pullout forces at the PDL-bone interface (Z1) prompting movement of the mineralized front into the PDL-space. Perpetuating loading can shift an original tension based zone to a compression zone specifically at Z3 **(B)**. The increased compression field in Z3 can cause cementum resorption in an attempt to maintain necessary PDL-space. However, it should be noted that the unequal turnover rates of bone and cementum tissues to a similar vector (magnitude and direction) is a fundamental that should be highlighted in explaining this model.

V: blood vessel; **T**: tooth; **B**: bone; **F**: Force; **Z1**: zone 1 corresponding to PDL-bone interfacial region; **Z2**: zone 2 corresponding predominantly to PDL; **Z3**: zone 3 corresponding to PDL-cementum interfacial region. Note: Zones Z1 and Z3 are proposed as strain amplified sites owing to PDL-soft tissue interaction with both hard tissues, i.e. bone and cementum respectively.